Featured in Physics

## **Experimental Determination of the Energy per Particle in Partially Filled Landau Levels**

Fangyuan Yang<sup>®</sup>, Alexander A. Zibrov, Ruiheng Bai<sup>®</sup>, Takashi Taniguchi, Kenji Watanabe, Michael P. Zaletel, and Andrea F. Young<sup>®</sup>,

<sup>1</sup>Department of Physics, University of California, Santa Barbara, California 93106, USA
<sup>2</sup>International Center for Materials Nanoarchitectonics, National Institute for Materials Science, 1-1 Namiki, Tsukuba 305-0044, Japan
<sup>3</sup>Research Center for Functional Materials, National Institute for Materials Science, 1-1 Namiki, Tsukuba 305-0044, Japan
<sup>4</sup>Department of Physics, University of California, Berkeley, California 94720, USA

(Received 13 August 2020; accepted 15 February 2021; published 13 April 2021)

We describe an experimental technique to measure the chemical potential  $\mu$  in atomically thin layered materials with high sensitivity and in the static limit. We apply the technique to a high quality graphene monolayer to map out the evolution of  $\mu$  with carrier density throughout the N=0 and N=1 Landau levels at high magnetic field. By integrating  $\mu$  over filling factor  $\nu$ , we obtain the ground state energy per particle, which can be directly compared to numerical calculations. In the N=0 Landau level, our data show exceptional agreement with numerical calculations over the whole Landau level without adjustable parameters as long as the screening of the Coulomb interaction by the filled Landau levels is accounted for. In the N=1 Landau level, a comparison between experimental and numerical data suggests the importance of valley anisotropic interactions and reveals a possible presence of valley-textured electron solids near odd filling.

DOI: 10.1103/PhysRevLett.126.156802

Partially filled Landau levels (LLs) are a paradigmatic example of flat band systems where dominant Coulomb interactions lead to a rich phase diagram of correlation driven electron states. Theoretically, the partially filled LL provides a compromise between phenomenological richness and computational tractability. However, quantitatively benchmarking numerical methods with transport measurements is typically limited to a discrete set of LL filling factors:  $\nu$ . Thermodynamic quantities such as the chemical potential  $\mu$  are more closely related to theoretically calculable quantities. Owing to recent progress in improving sample quality [1] and the fact that the single particle band structure is known to a high degree of accuracy, graphene is an ideal venue to pursue a quantitative understanding of partially filled LLs. In this Letter, we report precise measurements of  $\mu$  in a high quality monolayer graphene at zero and high magnetic fields. Typical measurements of thermodynamic quantities in graphene probe the compressibility  $\partial n/\partial \mu$  at finite frequency [2-5], hindering accurate measurements in the quantum Hall regime where equilibration times can become long. Our measurements probe  $\mu$  directly [6] in the static  $\omega \to 0$  limit. This allows us to determine  $\mu$  across a continuous range of  $\nu$  and subsequently the total energy per flux quantum E where  $\mu = \partial E/\partial \nu$ .

Our heterostructure consists of two graphene monolayers embedded between top and bottom graphite gates [see Figs. 1(a), 1(b) and Fig. S1 in the Supplemental Material [7]), with each conducting layer separated by a hexagonal boron nitride (hBN) dielectric of approximately 40 nm

thickness. The dual graphite-gated structure ensures low charge inhomogeneity on both graphene monolayers while allowing independent control of their respective carrier densities through the static gate voltages applied to the top gate  $(v_t)$ , bottom gate  $(v_b)$ , and top monolayer  $(v_d)$ . Internal contacts [21–25] are attached to the top monolayer—designated the "detector"—and are used to measure its bulk conductivity  $\sigma_d$ . To measure  $\mu$  of the bottom ("sample") graphene, we keep it grounded, and control  $\mu$  by sweeping  $v_b$ . For each fixed  $v_b$ , we adjust the  $v_t$  to null the effect of changes in  $\mu$  on the detector layer density. Under these conditions, the change in detector layer density  $\delta n_d = 0$  implies  $\delta \mu = -c_t \delta v_t/c_0$  [26].  $\delta \mu$  is then determined by recording  $\delta v_t$  and calibrating the geometric capacitance lever arm  $c_t/c_0$  (see Fig. S2).

Functionally,  $\delta n_d = 0$  is enforced by choosing a "target" density  $n_d$  such that  $\sigma_d$  is at a conductance minimum corresponding to the Dirac point at B=0 T or a weak fractional quantum Hall (FQH) state at high B. Figure 1(b) shows the schematic of our measurement circuit, which uses a digital feedback loop to maintain  $\sigma_d$  at its minimum as other parameters are swept. While the current measurement is done at finite frequency to allow low noise readout, it does not require charging of the sample layer at these frequencies. This allows us to access regimes where the sample layer conductivity is very small and equilibration times are very large. In practice, measurements are typically done with equilibration times of  $\tau \approx 1$  sec.

Figure 1(d) shows  $\mu$  measured at B = 0 T and 200 mT, plotted as a function of the sample carrier density

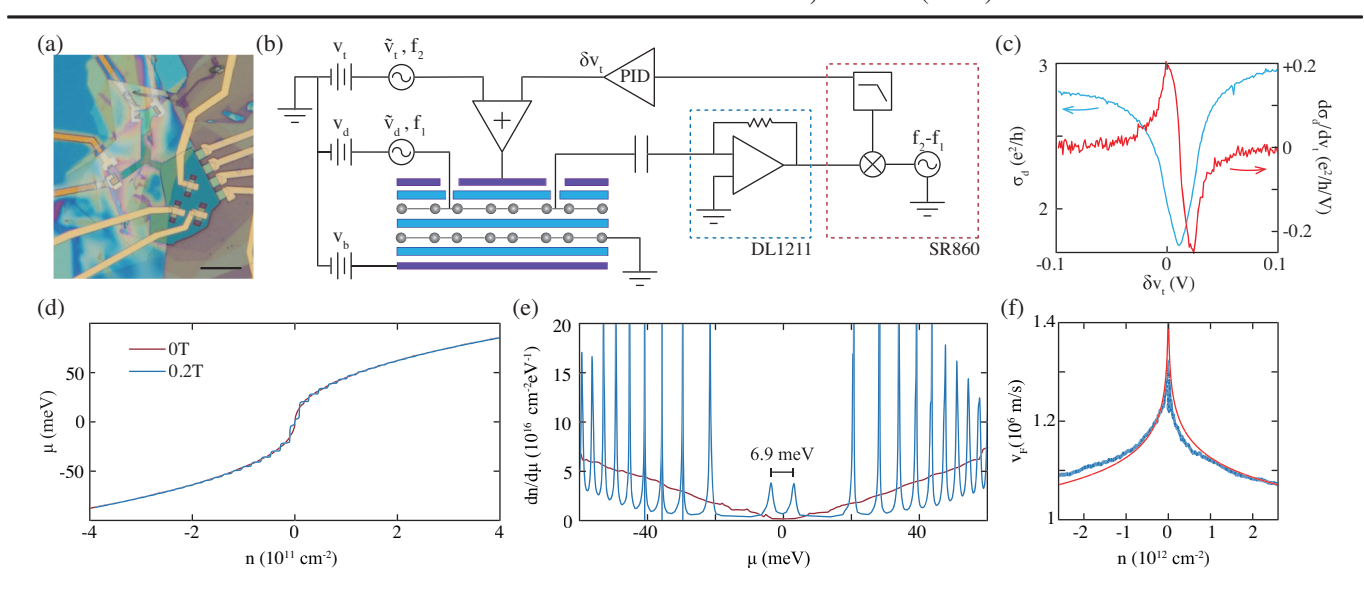


FIG. 1. Measurement setup. (a) Optical image of the device; scale bar is 10  $\mu$ m. (b) Measurement schematic. Static gate voltages are applied to the top gate  $(v_t)$ , bottom gate  $(v_b)$ , and detector monolayer  $(v_d)$ .  $\sigma_d$  is measured by applying an ac voltage  $\tilde{v}_d$  at frequency  $f_1=13.77$  Hz to one of the internal contacts and measuring the current at another with a DL1211 amplifier. An additional ac voltage  $(\tilde{v}_t)$  is applied to the top gate at  $f_2=110$  Hz. Demodulating the current at  $f_2-f_1$  with an SR860 lock-in amplifier produces a signal proportional to  $d\sigma_d/dv_t$ , which vanishes at a conductivity minimum independent of contact resistance. We use a feedback loop to continuously adjust a static voltage  $\delta v_t$  in order to maintain  $d\sigma_d/dv_t=0$ . Under these conditions,  $\delta \mu=-c_t\delta v_t/c_0$ . (c)  $\sigma_d$  (blue) and  $\delta \sigma_d/\delta v_t$  (red) as a function of  $\delta v_t$ . (d)  $\mu(n)$  at B=0 T (red) and 0.2 T (blue), measured at T=15 mK. (e) Density of states  $dn/d\mu$  calculated by numerical differentiation of data in panel (d). The ZLL is split by a sublattice gap [27,28] of  $\Delta_{AB}=6.9$  meV. (f) n-dependent  $v_F$  measured by fitting B=0 T data to  $\mu^2=(\Delta_{AB}/2)^2+(\hbar v_F\sqrt{\pi}|n|)^2$  with  $\Delta_{AB}$  fixed and  $v_F$  a free function of n. The red curve is a fit to theoretical models [29–31] of Fermi velocity renormalization by Coulomb interactions.

 $n = c_0(v_d - \mu) + c_b(v_b - \mu)$ , where  $c_b$  is the capacitance between the sample and the bottom gate.  $\mu(n)$  shows the  $\sqrt{n}$  dependence expected for the linearly dispersing bands of monolayer graphene [2], as well as steps associated with LL formation when a small magnetic field is applied. To quantitatively model the data, we take  $\mu^2 = (\Delta_{AB}/2)^2 +$  $(\hbar v_F \sqrt{\pi |n|})^2$ , where  $\Delta_{AB}$  is the sublattice splitting that arises mostly due to alignment of the graphene with one of the encapsulating hBN layers [27,28] and  $v_F$  is the Fermi velocity. We determine  $\Delta_{AB} = 6.9$  meV from the splitting of the zero energy LL (ZLL) centered at  $\mu = 0$ , which is evident in Fig. 1(e) where we plot  $dn(\mu)/d\mu$  as determined by numerical differentiation of the  $\mu(n)$  data (see also Fig. S3). Figure 1(f) shows  $v_F(n)$ , determined by fixing  $\Delta_{AB}$  but allowing  $v_F$  to be a free *n*-dependent parameter.  $v_F$  is enhanced at low densities, consistent with past experiments [32,33], and well fit by theoretical models of Fermi velocity renormalization [29–31], as shown by the red curve in Fig. 1(f) and described in the Supplemental Material [7].

The LLs of monolayer graphene are approximately fourfold degenerate due to the spin and valley degrees of freedom, but this degeneracy is spontaneously broken at high magnetic fields via quantum Hall ferromagnetism. Figure 2(a) presents  $\mu(\nu)$  at B=14 T across the ZLL that spans  $-2 < \nu < +2$ , where  $\nu = 2\pi\ell_B^2 n$  is the LL filling

factor. The high quality of the detector layer is crucial for achieving high experimental  $\mu$  resolution, as FQH conductivity minima in the detector layer provide sensitive transducers for the sample layer chemical potential (see Fig. S4). Over large regions of density,  $\mu(\nu)$  decreases as a function of  $\nu$  (negative compressibility) despite the naive expectation that  $\mu$  should increase monotonically with  $\nu$ due to Coulomb repulsion. The decrease occurs because the chemical potential measured here is actually relative to that of a classical capacitor, which subtracts off the q = 0 part of the Coulomb interaction  $\frac{1}{2}V(q=0)n^2$ . It is well understood [26,34] that negative compressibility then arises because correlations lower the energy of quantum Hall states relative to that of a uniform charge distribution.  $\mu$ jumps at each integer  $\nu$ , which indicates incompressible integer quantum Hall states arising from the broken symmetry of the spin and valley components of the isospin. Additional jumps are observed at a series of fractional  $\nu$ associated with incompressible FQH states at  $\nu^* =$  $p/(2p \pm 1)$  (p = 1, 2, 3, ...) and  $\nu^* = p/(4p \pm 1)$  (with p = 1 and 2) [3–5,35]. Here  $\nu^* = |\nu - \nu_0|$  indicates the filling relative to an adjacent integer filling  $\nu_0 \in \mathbf{Z}$ . At high B, the regions around integer  $\nu$  (shaded in blue) are good insulators and so are no longer accessible at low temperatures due to the hours-long or days-long equilibration time of the sample layer (see Fig. S5).

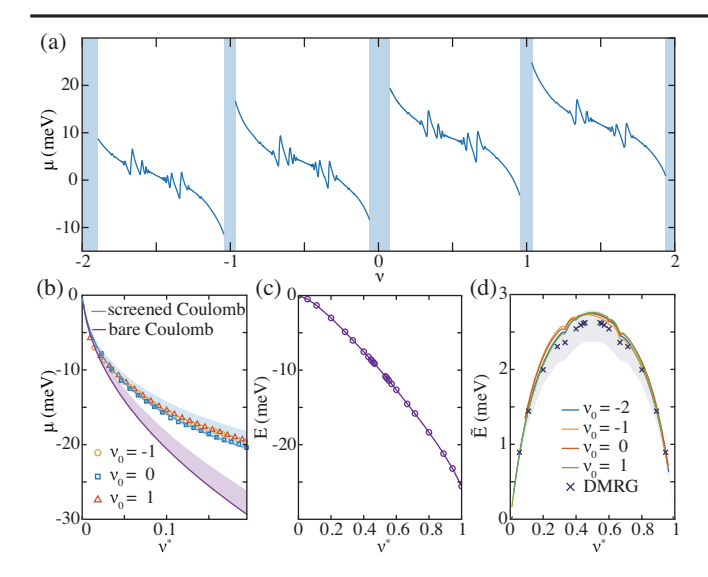


FIG. 2. Chemical potential and energy per flux quantum in the N = 0 LL. (a)  $\mu(\nu)$  within the ZLL measured at B = 14 T and nominal T=15 mK. Blue regions indicate domains of  $\nu$  where the charging time of the sample exceeds the measurement time of  $\sim 1$  sec (see Fig. S5). (b)  $\mu$  at B = 18 T and nominal T = 40 mK for low  $\nu^*$ , measured relative to  $\nu = -1$  (orange),  $\nu = 0$  (blue), and  $\nu = 1$  (red). The cyan and purple curves are calculated  $\mu$  for a Wigner crystal with screened and unscreened Coulomb interactions, respectively, taking  $\epsilon_{hBN} = 4.0$  and  $\alpha_G = 1.85$ ; shaded ranges reflect uncertainty in those parameters as described in main text. The data are offset so that  $\mu(\nu^*) = 0$ . (c) Numerically calculated [36] total ground state energy of the N = 0 LL after accounting for the screened Coulomb interactions. (d) Comparison of experimentally determined (solid lines) and numerically calculated (dark blue crosses)  $\tilde{E}$ . Both experimental and numerical data have a linear-in- $\nu^*$  background subtracted so that  $\tilde{E}$  vanishes at integer  $\nu^*$ . Data were taken at B = 18 T and T = 40 mK.

The four copies of the ZLL are nearly identical apart from an offset in chemical potential, suggesting that the LL is close to being fully spin and valley polarized at this magnetic field. This is expected based on the measured value of  $\Delta_{AB}$ , which splits the valley degree of freedom in the ZLL. In combination with the Zeeman energy, FQH physics is expected to be predominantly single component [24] in this regime of magnetic fields. We begin our quantitative analysis at low  $\nu^*$ where electron Wigner crystal phases [37,38] are the expected ground state. In transport measurements, the Wigner crystal manifests as a low-temperature insulator that undergoes a metal-insulator transition at finite temperature due to pinning of the crystal by weak disorder, as observed in GaAs/AlGaAs quantum wells [39] and more recently in graphene [40]. The largely classical nature of the correlations in this regime make thermodynamic modeling tractable, and quantitative agreement obtains between theory [41] and compressibility measurements in GaAs/AlGaAs quantum wells [26,35].

Figure 2(b) shows  $\mu$  plotted as a function of  $\nu^*$  near different integer fillings within the ZLL. For comparison,

we also show theoretical calculations of  $\mu$  in the Wigner crystal phase developed for the case of unscreened Coulomb interactions [38], where  $\mu(\nu^*) = -1.173 |\nu^*|^{1/2} E_C$ . Here  $E_C = (e^2)/(\epsilon_{\rm hBN}\ell_B)$  is the Coulomb energy. The model has only one parameter, the dielectric constant  $\epsilon_{\rm hBN} =$  $\sqrt{\epsilon^{\parallel}} \epsilon^{\perp}$ , which is the geometric average of the in-plane and out-of-plane dielectric constants of the hBN substrate.  $e^{\perp} = 3.0$  can be determined in situ, but  $e^{\parallel}$  is not precisely known, though it is thought to be  $\epsilon^{\parallel} \approx 6.6$  [42]. Even accounting for uncertainty in this parameter, the model does not agree with experiment. Quantitative agreement is achieved, however, by considering the screening of the Coulomb interactions by the graphite gates, which are accounted for using standard electrostatic calculations and by the filled Dirac sea, which we account for within the random phase approximation [43]. This approximation takes as an additional input parameter the graphene fine structure constant  $\alpha_G$ . Still treating the electrons as a classical Wigner crystal, we numerically evaluate the Madelung-type energy for the screened interaction  $V_{\rm scr}(r)$  to obtain  $\mu(\nu^*)$  [7]. To reflect uncertainty in the input parameters, we show a range spanning  $\epsilon_{\text{hBN}} \in (4.0, 4.5)$  and  $\alpha_G \in (1.75, 2.2)$ , in addition to reference curves for  $\epsilon_{\rm hBN}=4.0$  and  $\alpha_G=1.85$ .

The screened Coulomb interaction provides an exceptionally good match to the experimental data, suggesting that no additional effects are present and that accounting for the screening is sufficient to achieve a quantitative understanding of this regime. We note that based on spin-wave transmission measurements [40], spin skyrmions appear to play a role in the Wigner solid phases near  $\nu=\pm 1$ . We do observe a small but systematic discrepancy between  $\mu$  near even and odd integer  $\nu$  in the Wigner crystal regime. This suggests that the large Zeeman energy,  $E_Z\approx 0.03E_C$ , restricts the skyrmion size to the point where they do not generate significant corrections to  $\mu$  at low  $\nu^*$ .

Closer to the center of the LL, correlations become quantum in nature and even numerical calculation of  $\mu$  is not tractable for arbitrary  $\nu$ . However, numerical methods can accurately calculate the "total energy" per flux quantum  $E(\nu)$  at many rational values of  $\nu$ , as has long been the focus of exact diagonalization and density matrix renormalization group (DMRG) studies. Figure 2(c) shows the ground state energy calculated using infinite DMRG [36] (iDMRG) on a circumference  $L=18\ell_B$  cylinder for a number of rational  $\nu$ , assuming wave functions are restricted to a single spin and valley component and making use of the screened interaction  $V_{\rm scr}$ .

The calculated E is dominated by a linear background,  $\mu_0\nu^*$ , that is proportional to the exchange-correlation energy of the integer quantum Hall effect; the correlations underlying the FQH effect are reflected in the deviations of the calculated E from this background. In Fig. 2(d), we subtract off the linear contribution by instead plotting  $\tilde{E} = E - \nu^* E(\nu^* = 1)$  [Fig. 2(d)], which ensures  $\tilde{E}(0) = \tilde{E}(1) = 0$ . This can be compared to experiment by

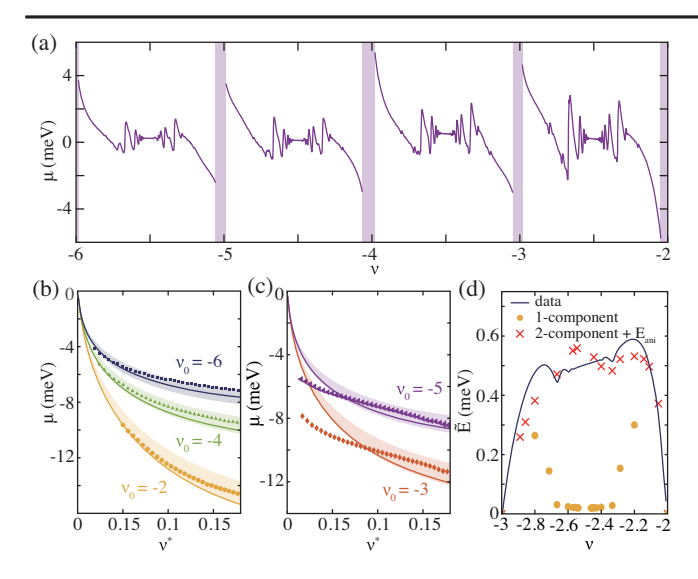


FIG. 3. Multicomponent effect and lattice scale interaction in the N=1 LL. (a)  $\mu$  in the N=1 LL at T=15 mK and B=13 T. (b)  $\mu$  measured near  $\nu_0=-2$ , -4, and -6. Solid lines are  $\mu$  calculated from the Wigner crystal model with parameters identical to those used in Fig. 2(b). (c)  $\mu$  near  $\nu_0=-3$  and -5. The solid lines showing the Wigner crystal model do not match the data, suggesting the importance of valley merons [44] near these fillings. (d) Comparison of experimentally determined  $\tilde{E}$  with numerical simulations for  $-3 < \nu < -2$ . One-component numerical calculations underestimate the experimental result by a significant margin. Including both valley components as well as the contribution of lattice scale anisotropies as in Eq. (1) with  $g_z=g_{xy}=0.1(a/\ell_B)E_C$  can restore agreement to within  $100 \ \mu eV \approx 2.5 \times 10^{-3}E_C$ .

integrating  $\mu(\nu)$ ,  $\tilde{E}(\nu^*) = \int_0^{\nu^*} [\mu(\nu) - \mu_0] d\nu$ , where  $\mu_0$  is chosen to ensure  $\tilde{E}(0) = \tilde{E}(1) = 0$ . To aid in fixing  $\mu_0$  accurately, the experimental data is extrapolated to integer  $\nu$  by using the Wigner crystal model. Numerical and experimental data agree to within experimental uncertainty in  $\alpha_G$  and  $\epsilon_{\rm hBN}$  without additional adjustable parameters. Similarly, the measured thermodynamic gap at charge neutrality 53 meV agrees with the theoretically calculated jump in  $\mu$  to within 4% [7]. These results constitute a remarkably good quantitative agreement for a many-body system.

Figure 3(a) shows  $\mu$  measured across the first excited LL, corresponding to orbital quantum number N=1 and spanning  $\nu \in (-6,-2)$ . In contrast to the N=0 level, both the size of the chemical potential jumps associated with FQH gaps [24] and the magnitude of the negative compressibility systematically decrease with increasing  $|\nu|$ . This trend arises naturally due to the nature of the screened Coulomb interaction  $V_{\rm scr}$  [43]: in the ZLL, particle-hole symmetry makes the screening  $\nu$  independent, but within the N=1 LL screening smoothly interpolates between the N=0 and N=2 values as the four-component LL fills. Indeed, applying this interpolation to the Wigner crystal regime near even filling factors produces an excellent quantitative match between the data and theory [Fig. 3(b)].

The N = 1 LL and ZLL are further distinguished by the effect of the sublattice symmetry breaking  $\Delta_{AB}$ , which splits the valleys in the ZLL but has negligible effect on the energies of the N=1 LL. This manifests most obviously in our data in the low- $\nu^*$  regimes around near odd integer filling, shown in Fig. 3(c). In contrast to the comparable regimes of  $\nu^*$  near even integers, and throughout the ZLL, the data are not matched by the predictions of  $V_{\rm scr}$  for a single electron Wigner crystal. To understand this data, we note that tilted field magnetotransport experiments [45] find evidence for a spin polarized state at  $\nu = \pm 4$  in which excitations are either single spin flips or small skyrmions similar to the situation at  $\nu = \pm 1$  in the ZLL. At  $\nu = \pm 3, \pm 5$ , in contrast, activated gaps show minimal tilted field dependence, which is consistent with the lowest energy charged excitations being valley textures. Theoretically, the ground state of a spin-polarized but valley-unpolarized LL applicable to  $\nu = \pm 3, \pm 5$  is then expected to be a solid of such valley textures [44], with resulting corrections to E and consequently to  $\mu$ . Notably, the corrections to the energy will be largest when the valley textures are most extended. The observed anomalous  $\mu(\nu)$ supports the idea that the low single-particle valley anisotropy in the N = 1 LL stabilizes a solid of extended valley textures. This could be tested in the future by extending numerical calculations [44] of such solids to include the screened Coulomb interaction.

The multicomponent nature of the N = 1 LL is further evidenced in Fig. 3(d), where iDMRG simulations of a single component system fail to reproduce the experimentally determined  $\tilde{E}$  when using the same model parameters that produce good agreement in the ZLL. Interestingly, iDMRG finds a significantly lower total energy compared to experiment. This suggests a missing contribution to the energy, since adding degrees of freedom to a variational parameter space can only lower the numerically calculated energy, increasing the discrepancy. An appealing candidate is the anisotropy of the Coulomb interactions at small length scales, which breaks the valley-SU(2) symmetry and can be expected to provide corrections of  $E_{\rm ani} \sim$  $(a/\ell_B)E_C \approx 1.75$  meV at B = 13 T, where a = 0.246 nm is the graphene lattice constant. Though known to be important in the ZLL [1] near  $\nu = 0$ , evidence for shortrange anisotropy in the N = 1 LL has been limited to the observation of a possible valley-ordered state at  $\nu = 4$  for low magnetic fields [24], and they have not received much attention in the theoretical literature [46,47].

To model their effect, we analyze the interactions that arise when projecting a short-range Hubbard-U interaction into the N=1 LL. For simplicity we assume full-spin polarization so that electrons are described by a two-component field  $\psi_r$  indexed by valley  $\tau^z$ . It is convenient to express the result as the continuum interaction that would produce the same Hamiltonian if the electrons were in the N=0 LL. Taking into account the interplay of the

form factors of the N = 1 LL and the sublattice structure, we find the general form [7]

$$\begin{split} H_{\rm ani} &= \frac{1}{2} \int d^2 r_{1/2} [g_z \psi_{r_1}^{\dagger} \tau^z \psi_{r_1} \ell_B^4 \nabla^4 \delta(r_1 - r_2) \psi_{r_2}^{\dagger} \tau^z \psi_{r_2} \\ &+ g_{xy} \psi_{r_1}^{\dagger} \tau^x \psi_{r_1} \ell_B^2 \nabla^2 \delta(r_1 - r_2) \psi_{r_2}^{\dagger} \tau^x \psi_{r_2} + (x \to y)], \end{split}$$

$$(1)$$

where  $g_i \sim (a/\ell_B)E_c$ . Note that the interactions are *derivatives* of  $\delta$  functions; in contrast, the same exercise in the ZLL would find contact interactions [47,48]. Because the FQH effect around density  $\nu^* = \frac{1}{m}$  attaches zeros  $(z_i - z_j)^m$  to the interelectron wave function, a  $\nabla^{2m}\delta$  interaction effectively "turns off" for densities below  $\frac{1}{m+1}$ . In the ZLL, this means the anisotropies only operate for  $-1 < \nu < 1$ , while in the N=1 we predict the anisotropies act for all  $2+1/3 < \nu < 6-1/3$ . This is indeed the region where our one-component numerics deviate from experiment.

Treating  $g_z$ ,  $g_{xy}$  as adjustable phenomenological parameters, we perform two-component iDMRG numerics that include  $H_{\rm ani}$ . Figure 3(d) shows the results for  $g_{xy}=g_z=0.1(a/\ell_B)E_C$ , which agree with experiment to within 100  $\mu{\rm eV}$ , comparable to the discrepancies observed in the ZLL. In both LLs, these discrepancies amount to  $2\times 10^{-3}$  of the bare Coulomb energy  $E_C$ .

In conclusion, we have developed an experimental technique to measure  $\mu$  to high precision in van der Waals heterostructures and applied it to high-quality graphene monolayers in the fractional quantum Hall regime, achieving remarkable agreement between experiment and numerical many-body simulations. Our technique paves the way for measuring thermodynamic quantities, such as entropy, which may shed light on more subtle questions such as those related to quasiparticle statistics [49].

M. P. Z. acknowledges conversations with M. Ippoliti, Z. Papic, N. Regnault, and E. Rezayi, who generously provided exact-diagonalization energies, as well as M. Metlitski. The iDMRG code used in this work was developed in collaboration with R. Mong and F. Pollmann. F. Y. and R. B. acknowledge experimental assistance by H. Zhou. F. Y. acknowledges discussions with H. Polshyn and C. Tschirhart. Experimental work by F. Y., A. A. Z., R. B., and A. F. Y. was supported by the National Science Foundation under DMR-1654186. Work by M.P.Z. is supported by the Army Research Office under W911NF-17-1-0323. A portion of this work was performed at the National High Magnetic Field Laboratory, which is supported by the National Science Foundation Cooperative Agreement No. DMR-1644779 and the State of Florida. K. W. and T. T. acknowledge support from the Elemental Strategy Initiative conducted by the MEXT, Japan (Grant No. JPMXP0112101001), JSPS KAKENHI (Grant No. JP20H00354), and the CREST (JPMJCR15F3), JST. A. F. Y. acknowledges the support of the David and Lucile Packard Foundation.

- \*Corresponding author. andrea@physics.ucsb.edu
- [1] C. Dean, P. Kim, J. I. A. Li, and A. Young, in *Fractional Quantum Hall Effects: New Developments* (World Scientific, Singapore, 2020), pp. 317–375.
- [2] J. Martin, N. Akerman, G. Ulbricht, T. Lohmann, J. H. Smet, K. von Klitzing, and A. Yacoby, Nat. Phys. 4, 144 (2008).
- [3] B. E. Feldman, B. Krauss, J. H. Smet, and A. Yacoby, Science **337**, 1196 (2012).
- [4] B. E. Feldman, A. J. Levin, B. Krauss, D. A. Abanin, B. I. Halperin, J. H. Smet, and A. Yacoby, Phys. Rev. Lett. 111, 076802 (2013).
- [5] A. A. Zibrov, E. M. Spanton, H. Zhou, C. Kometter, T. Taniguchi, K. Watanabe, and A. F. Young, Nat. Phys. 14, 930 (2018).
- [6] K. Lee, B. Fallahazad, J. Xue, D. C. Dillen, K. Kim, T. Taniguchi, K. Watanabe, and E. Tutuc, Science 345, 58 (2014).
- [7] See Supplemental Material at http://link.aps.org/supplemental/10.1103/PhysRevLett.126.156802 for more details about device fabrication, characterization, and theoretical models, which includes Ref. [8–20].
- [8] J. Zhu, H. L. Stormer, L. N. Pfeiffer, K. W. Baldwin, and K. W. West, Phys. Rev. B 61, R13361 (2000).
- [9] E. Tutuc, R. Pillarisetty, S. Melinte, E. P. De Poortere, and M. Shayegan, Phys. Rev. B 68, 201308(R) (2003).
- [10] W. Pan, J. L. Reno, and J. A. Simmons, Phys. Rev. B 71, 153307 (2005).
- [11] S. Misra, N. C. Bishop, E. Tutuc, and M. Shayegan, Phys. Rev. B 78, 035322 (2008).
- [12] A. Usher and M. Elliott, J. Phys. Condens. Matter 21, 103202 (2009).
- [13] N. Ruhe, G. Stracke, C. Heyn, D. Heitmann, H. Hardtdegen, T. Schäpers, B. Rupprecht, M. A. Wilde, and D. Grundler, Phys. Rev. B 80, 115336 (2009).
- [14] L. H. Ho, L. J. Taskinen, A. P. Micolich, A. R. Hamilton, P. Atkinson, and D. A. Ritchie, Phys. Rev. B 82, 153305 (2010)
- [15] J. Pollanen, J. P. Eisenstein, L. N. Pfeiffer, and K. W. West, Phys. Rev. B 94, 245440 (2016).
- [16] I. F. Herbut, Phys. Rev. B 75, 165411 (2007).
- [17] J. Jung and A. H. MacDonald, Phys. Rev. B **80**, 054416 (2009).
- [18] K. Nomura, S. Ryu, and D.-H. Lee, Phys. Rev. Lett. **103**, 216801 (2009).
- [19] D. V. Khveshchenko, Phys. Rev. Lett. **87**, 206401 (2001).
- [20] A. F. Young, J. D. Sanchez-Yamagishi, B. Hunt, S. H. Choi, K. Watanabe, T. Taniguchi, R. C. Ashoori, and P. Jarillo-Herrero, Nature (London) 505, 528 (2014).
- [21] J. Yan and M. S. Fuhrer, Nano Lett. 10, 4521 (2010).

- [22] Y. Zhao, P. Cadden-Zimansky, F. Ghahari, and P. Kim, Phys. Rev. Lett. 108, 106804 (2012).
- [23] M. J. Zhu, A. V. Kretinin, M. D. Thompson, D. A. Bandurin, S. Hu, G. L. Yu, J. Birkbeck, A. Mishchenko, I. J. Vera-Marun, K. Watanabe, T. Taniguchi, M. Polini, J. R. Prance, K. S. Novoselov, A. K. Geim, and M. Ben Shalom, Nat. Commun. 8, 14552 (2017).
- [24] H. Polshyn, H. Zhou, E. M. Spanton, T. Taniguchi, K. Watanabe, and A. F. Young, Phys. Rev. Lett. 121, 226801 (2018).
- [25] Y. Zeng, J. I. A. Li, S. A. Dietrich, O. M. Ghosh, K. Watanabe, T. Taniguchi, J. Hone, and C. R. Dean, Phys. Rev. Lett. 122, 137701 (2019).
- [26] J. P. Eisenstein, L. N. Pfeiffer, and K. W. West, Phys. Rev. Lett. 68, 674 (1992).
- [27] B. Hunt, J. D. Sanchez-Yamagishi, A. F. Young, M. Yankowitz, B. J. LeRoy, K. Watanabe, T. Taniguchi, P. Moon, M. Koshino, P. Jarillo-Herrero, and R. C. Ashoori, Science 340, 1427 (2013).
- [28] F. Amet, J. R. Williams, K. Watanabe, T. Taniguchi, and D. Goldhaber-Gordon, Phys. Rev. Lett. 110, 216601 (2013).
- [29] J. González, F. Guinea, and M. A. H. Vozmediano, Phys. Rev. B 59, R2474 (1999).
- [30] S. Das Sarma, E. H. Hwang, and W.-K. Tse, Phys. Rev. B **75**, 121406(R) (2007).
- [31] M. Polini, R. Asgari, Y. Barlas, T. Pereg-Barnea, and A. H. MacDonald, Solid State Commun. 143, 58 (2007).
- [32] D. C. Elias, R. V. Gorbachev, A. S. Mayorov, S. V. Morozov, A. A. Zhukov, P. Blake, L. A. Ponomarenko, I. V. Grigorieva, K. S. Novoselov, F. Guinea, and A. K. Geim, Nat. Phys. 7, 701 (2011).
- [33] J. Chae, S. Jung, A. F. Young, C. R. Dean, L. Wang, Y. Gao, K. Watanabe, T. Taniguchi, J. Hone, K. L. Shepard, P. Kim,

- N. B. Zhitenev, and J. A. Stroscio, Phys. Rev. Lett. 109, 116802 (2012).
- [34] G. Fano, F. Ortolani, and E. Colombo, Phys. Rev. B 34, 2670 (1986).
- [35] J. P. Eisenstein, L. N. Pfeiffer, and K. W. West, Phys. Rev. B 50, 1760 (1994).
- [36] M. P. Zaletel, R. S. K. Mong, F. Pollmann, and E. H. Rezayi, Phys. Rev. B 91, 045115 (2015).
- [37] P.K. Lam and S.M. Girvin, Phys. Rev. B **30**, 473 (1984).
- [38] D. Levesque, J. J. Weis, and A. H. MacDonald, Phys. Rev. B 30, 1056 (1984).
- [39] V. J. Goldman, M. Santos, M. Shayegan, and J. E. Cunningham, Phys. Rev. Lett. 65, 2189 (1990).
- [40] H. Zhou, H. Polshyn, T. Taniguchi, K. Watanabe, and A. F. Young, Nat. Phys. 16, 154 (2019).
- [41] L. Bonsall and A. A. Maradudin, Phys. Rev. B 15, 1959 (1977).
- [42] R. Geick, C. H. Perry, and G. Rupprecht, Phys. Rev. 146, 543 (1966).
- [43] K. Shizuya, Phys. Rev. B 75, 245417 (2007).
- [44] R. Côté, J.-F. Jobidon, and H. A. Fertig, Phys. Rev. B 78, 085309 (2008).
- [45] A. F. Young, C. R. Dean, L. Wang, H. Ren, P. Cadden-Zimansky, K. Watanabe, T. Taniguchi, J. Hone, K. L. Shepard, and P. Kim, Nat. Phys. 8, 550 (2012).
- [46] J. Alicea and M. P. A. Fisher, Phys. Rev. B 74, 075422 (2006).
- [47] M. Kharitonov, Phys. Rev. B 85, 155439 (2012).
- [48] I. Sodemann and A. H. MacDonald, Phys. Rev. Lett. 112, 126804 (2014).
- [49] N. R. Cooper and A. Stern, Phys. Rev. Lett. 102, 176807 (2009).